The Astrophysical Journal Supplement Series, 280:47 (7pp), 2025 October https://doi.org/10.3847/1538-4365/adfc68

Precise Frequencies of $H_2{}^{16}O$ Lines Protected for Radio Astronomy

Arthémise Altman[1], Roland Tóbiás[2,3], Alexandr S. Bogomolov[1], Meissa L. Diouf[4], Frank M. J. Cozijn[4], Attila G. Császár[3], Clément Lauzin[1], and Wim Ubachs[4]
[1] Institute of Condensed Matter and Nanosciences, Université catholique de Louvain, Louvain-la-Neuve, Belgium
[2] Department of Chemistry, University of Vermont, Burlington, VT 05405, USA; roland.tobias@ttk.elte.hu
[3] Institute of Chemistry, ELTE Eötvös Loránd University, H-1117 Budapest, Pázmány Péter sétány 1/A, Hungary
[4] Department of Physics and Astronomy, LaserLaB, Vrije Universiteit, De Boelelaan 1100, 1081 HZ Amsterdam, The Netherlands; w.m.g.ubachs@vu.nl
Received 2025 June 26; revised 2025 August 13; accepted 2025 August 14; published 2025 September 15

Abstract

Precise frequency values have been determined for $H_2{}^{16}O$ radio lines appearing in protected line lists of the International Astronomical Union and the Panel on Frequency Allocations of the US National Academy of Sciences. The improved precision is attributable to a spectroscopic network built from a large set of near-infrared Lamb-dip lines augmented with a handful of ultra-high-accuracy rotational transitions. The ultraprecise $H_2{}^{16}O$ network contains 376 Lamb-dip lines recorded previously via our frequency-comb-locked cavity-enhanced spectrometer. During the present study, a total of 55 target lines have been (re)measured at high accuracy. Due to our network-assisted measurements, the accuracy has been significantly improved with respect to previous direct radio-frequency measurements for all the protected lines of $H_2{}^{16}O$ above 750 GHz. Furthermore, 43 of these protected transitions now benefit from the accuracy of the new near-infrared Lamb dips reported in this paper.

Unified Astronomy Thesaurus concepts: Radio astronomy (1338)

1. Introduction

The water molecule, H_2O, is one of the key species throughout the Universe. It is made up of hydrogen, the most abundant element produced primordially, and oxygen, the third most abundant element produced in supernovae (E. F. van Dishoeck et al. 2013). Water molecules are synthesized in either gas-phase interactions (P. Solomon & W. Klemperer 1972) or via solid-state processes (A. Tielens & W. Hagen 1982) in interstellar space.

Water in the interstellar medium was discovered in the early days of radio astronomy (A. C. Cheung et al. 1969) through a 22 GHz maser line. Since then, the presence of water has been investigated via radio astronomical observations of the interstellar medium under various conditions (C. M. Wright et al. 2000; J. Cernicharo et al. 2006), using maser transitions as well as thermal spectral lines. In pushing the limits of radio astronomy, water was observed at a redshift of $z = 5.6$ (A. Weiß et al. 2013).

Data sets for reference frequencies of many molecular transitions, including those of $H_2{}^{16}O$, are maintained in numerous databases. In terms of radio astronomy, the most relevant data banks appear to be the Cologne Database for Molecular Spectroscopy (CDMS)[5] (H. S. P. Müller et al. 2005; C. P. Endres et al. 2016) and the Jet Propulsion Laboratory (JPL) line catalog[6] (H. Pickett et al. 1998).

At the 21st General Assembly of the International Astronomical Union (IAU), taking place in Buenos Aires (1991 July 23–August 1), the astronomically most important spectral lines were carefully reviewed. The need to protect the frequencies of these lines with some minimally line-specific bandwidths was defined. The original list covered 73 lines, of which four pertain to $H_2{}^{16}O$. Later, in preparation for the World Radiocommunication Conference 2000, held in Istanbul (2000 May 8–June 2), the IUCAF (Scientific Committee on Frequency Allocations for Radio Astronomy and Space Science) millimeter wavelengths working group examined all known transitions in this region and specified revised allocations above 71 GHz. This catalog supplements the earlier list constructed by the IAU, extends it to 1 THz, and covers in total 13 lines for $H_2{}^{16}O$. Both collections can be accessed digitally.[7] Fifteen years later, the Panel on Frequency Allocations and Spectrum Protection for Scientific Uses of the US National Academy of Sciences (Committee on Radio Frequencies Board on Physics and Astronomy, National Academies of Sciences–Engineering–Medicine 2015) extended the list of protected water lines, in particular covering the frequency window between 1 and 3 THz, with 47 lines for $H_2{}^{16}O$ (here referred to as the NAS list). This leads to, altogether, 60 protected lines for this isotopologue.

The principal aim of this investigation is to provide frequency estimates with improved accuracy for the overwhelming majority of these 60 lines. To achieve this goal, laser-based precision spectroscopy measurements were conducted for dozens of carefully chosen near-infrared transitions in the 1.2–1.4 μm range. Based on all the new and old kHz-accuracy transitions available for $H_2{}^{16}O$, an ultraprecise spectroscopic network (A. G. Császár & T. Furtenbacher 2011) was assembled, delivering highly accurate energies for 79 pure rotational states.

As shown in W. Ubachs et al. (2024), such ultraprecise spectroscopic networks facilitate the extraction of highly accurate frequencies for radio lines. In that study, the existing ultraprecise $H_2{}^{16}O$ and $H_2{}^{18}O$ networks were extended with newly measured Lamb-dip lines, enabling the derivation of

[5] https://cdms.astro.uni-koeln.de/
[6] https://spec.jpl.nasa.gov/
[7] http://www.craf.eu/iau-list-of-important-spectral-lines/

accurate frequencies for a list of $H_2{}^{16}O$ maser transitions, as well as $H_2{}^{18}O$ lines observed extragalactically. Following this approach, the present work provides significantly refined frequency predictions for the protected $H_2{}^{16}O$ transitions, enhancing their reliability for future astronomical applications. The precise frequencies may find application in the accurate determination of velocities in astrophysical environments (G. Cazzoli et al. 2004).

2. Ultraprecise $H_2{}^{16}O$ Network

As to the notation used for the rovibrational states of $H_2{}^{16}O$, the vibrations are labeled with a triplet of normal-mode quantum numbers, (v_1, v_2, v_3), where v_1, v_2, and v_3 represent the symmetric stretch, bend, and antisymmetric stretch motions, respectively. For the rotations, the rigid-rotor asymmetric-top quantum numbers J, K_a, and K_c are employed in the form J_{K_a,K_c}. The rovibrational assignment of a transition is given here as $(v_1' \, v_2' \, v_3')J'_{K_a',K_c'} \leftarrow (v_1'' \, v_2'' \, v_3'')J''_{K_a'',K_c''}$, where $'$ and $''$ stand for its upper and lower states, respectively. Throughout the whole paper, only standard NIST/SEMATECH (2012) uncertainties will be used.

In this study, the spectroscopic-network-assisted precision spectroscopy (SNAPS) procedure (R. Tóbiás et al. 2020) was applied to determine a large number of accurate transition frequencies, involving newly measured near-infrared Lamb-dip lines to form energy differences. These Lamb dips were recorded via laser-based Doppler-free saturation spectroscopy, yielding frequency uncertainties down to the kHz level. The superior sensitivity of the noise-immune cavity-enhanced optical-heterodyne molecular spectroscopy (NICE-OHMS) method (L. Gianfrani et al. 2024) is well suited to detecting weak lines, whose lower states have small population densities at room temperature. When combined with frequency-comb calibration, NICE-OHMS is suitable for providing absolute accuracy for the measured line positions.

In our previous experimental campaigns (R. Tóbiás et al. 2020; M. L. Diouf et al. 2022b; R. Tóbiás et al. 2024; W. Ubachs et al. 2024), several hundred $H_2{}^{16}O$ Lamb dips were measured, involving rovibrational states within polyads $P = 0$, 1, 4, and 5, where $P = 2v_1 + v_2 + 2v_3$ is the polyad number. Note, in particular, that ultra-high-accuracy energies could be deduced for so-called hubs (that is, quantum states holding very large numbers of transitions) in the full experimental $H_2{}^{16}O$ spectroscopic network (T. Furtenbacher et al. 2020a, 2020b) available at that time (R. Tóbiás et al. 2024).

From the perspective of rovibrational spectroscopy, the quantum states of the $H_2{}^{16}O$ species, containing two equivalent hydrogen atoms with a nuclear spin of $I = 1/2$, fall into four subnetworks. The para-$H_2{}^{16}O$ levels, with a total nuclear spin of $I = 0$, are fully separated from the ortho-$H_2{}^{16}O$ states, with $I = 1$, and no transitions between the states of these nuclear-spin isomers have ever been detected (A. Miani & J. Tennyson 2004). The para- and ortho-$H_2{}^{16}O$ levels are defined by $(-1)^{v_3+K_a+K_c}$ being $+1$ or -1, respectively. Within the (0 0 0) vibrational state, levels of opposite (total) parity cannot be linked via near-infrared dipole lines (note that even/odd-parity states have even/odd K_c values). Thus, when building a network from them, the even- and odd-parity subnetworks must be connected by pure rotational transitions.

One of the key features of spectroscopic networks is that their transitions form so-called paths and cycles (i.e., a series of connected lines, where the starting and ending states are different and identical, respectively). Paths are highly useful as they define energy differences between their starting and ending states, along with uncertainty estimates. Cycles help not only to confirm the internal accuracy of the measurements, but also to check the self-consistency of the assignments. For details, see Section 4 of W. Ubachs et al. (2024).

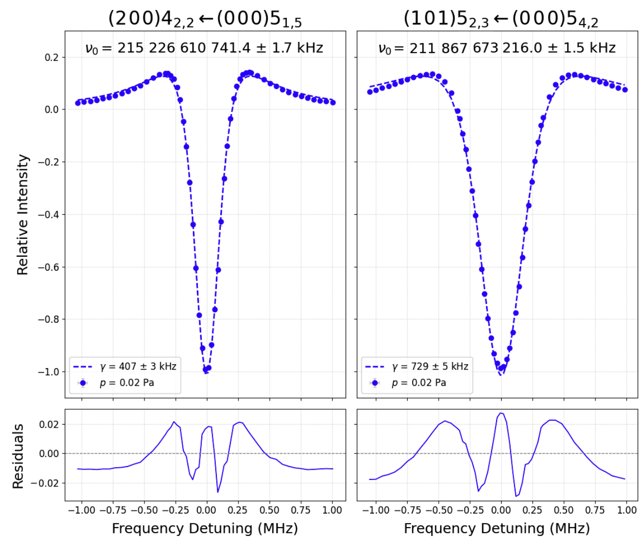

Figure 1. Examples for rovibrational Lamb-dip spectra measured for $H_2{}^{16}O$ using our NICE-OHMS setup. The γ parameters represent the full width at half maximum of the fitted Lorentzians, and p the pressure. The frequency detuning is relative to the observed frequency, ν_0 (see also Table 1).

In the ultraprecise network built for $H_2{}^{16}O$, several microwave (S. G. Kukolich 1969; G. Y. Golubiatnikov et al. 2006; G. Cazzoli et al. 2009) and near-infrared (J. Chen et al. 2018; S. Kassi et al. 2018; R. Tóbiás et al. 2020; M. L. Diouf et al. 2022b; S. Kassi et al. 2022; R. Tóbiás et al. 2024; W. Ubachs et al. 2024) transitions have been included. Following its latest update (W. Ubachs et al. 2024), this network now contains 411 previously measured microwave and near-infrared lines, where all the ortho (para) transitions form a single ortho (para) component.

3. NICE-OHMS Measurement Campaigns

To deduce kHz-accuracy frequencies for the protected $H_2{}^{16}O$ lines, an appropriately selected set of near-infrared lines was recorded using our NICE-OHMS setup at room temperature. The first parts of the experiments were performed at LaserLaB Amsterdam, with the NICE-OHMS spectrometer developed there (F. M. J. Cozijn et al. 2018; R. Tóbiás et al. 2020). This setup was later moved to Louvain-la-Neuve, where the UCLouvain laboratory served as the site for the second set of measurements.

In the Amsterdam campaign, statistical averaging was carried out over four recordings per line. The frequency metrology was based on beat-note measurements against a frequency-comb laser (Menlo Systems, FC1500), stabilized to a Cs clock (Microsemi CSIII), and long-term disciplined with respect to the Global Positioning System. This yielded a frequency scale with negligible uncertainties compared to the statistical errors. The pressure-shift uncertainties were estimated using a worst-case pressure slope, found to be ±20 kHz Pa^{-1} in our previous SNAPS studies (R. Tóbiás et al.

Table 1
New Near-infrared Lamb-dip Lines Measured Using an Ultrasensitive NICE-OHMS Spectrometer for $H_2{}^{16}O$

NICE-OHMS (This Work)[a]		Rovibrational Assignment[b]	Previous Results[c]		
Line Frequency (kHz)	p (Pa)		Dev.	Unc.	Reference
209,966,584,532.4 ± 1.4	0.02	$(1\,0\,1)3_{1,3} \leftarrow (0\,0\,0)4_{3,2}$	–300	3000	S. N. Mikhailenko et al. (2018)
210,038,636,486.7 ± 1.4	0.02	$(2\,0\,0)5_{0,5} \leftarrow (0\,0\,0)5_{3,2}$	–3.7	10.4	R. Tóbiás et al. (2024)
210,463,484,645.5 ± 1.5	0.02	$(0\,2\,1)6_{3,4} \leftarrow (0\,0\,0)6_{1,5}$	500	3000	S. N. Mikhailenko et al. (2018)
210,664,080,420.2 ± 1.3	0.02	$(0\,2\,1)6_{5,1} \leftarrow (0\,0\,0)7_{3,4}$	–21,800	3000	S. N. Mikhailenko et al. (2018)
211,120,145,834.0 ± 1.5	0.02	$(2\,0\,0)5_{4,2} \leftarrow (0\,0\,0)5_{5,1}$	–5.2	3.0	W. Ubachs et al. (2024)
211,126,350,475.9 ± 1.5	0.02	$(2\,0\,0)5_{4,1} \leftarrow (0\,0\,0)5_{5,0}$	–0.3	11.1	R. Tóbiás et al. (2024)
211,545,072,422.8 ± 1.5	0.02	$(1\,0\,1)2_{1,1} \leftarrow (0\,0\,0)3_{3,0}$	–0.8	7.5	R. Tóbiás et al. (2024)
211,630,806,780.1 ± 0.6	0.02	$(0\,2\,1)6_{3,4} \leftarrow (0\,0\,0)5_{3,3}$	100	3000	S. N. Mikhailenko et al. (2018)
211,802,311,374.9 ± 1.4	0.02	$(2\,0\,0)6_{3,4} \leftarrow (0\,0\,0)6_{4,3}$	–9.6	10.0	R. Tóbiás et al. (2024)
211,867,673,216.0 ± 1.5	0.02	$(1\,0\,1)5_{2,3} \leftarrow (0\,0\,0)5_{4,2}$	–0.2	7.7	R. Tóbiás et al. (2024)
212,286,960,311.8 ± 1.4	0.02	$(2\,0\,0)6_{3,3} \leftarrow (0\,0\,0)6_{4,2}$	2.5	10.4	R. Tóbiás et al. (2024)
212,549,726,956.5 ± 1.5	0.02	$(2\,0\,0)4_{2,3} \leftarrow (0\,0\,0)5_{1,4}$	1.3	7.5	M. L. Diouf et al. (2022b)
212,843,780,340.2 ± 1.4	0.02	$(2\,0\,0)5_{1,5} \leftarrow (0\,0\,0)5_{2,4}$	3.2	7.6	M. L. Diouf et al. (2022b)
212,877,518,672.9 ± 1.8	0.02	$(1\,0\,1)3_{1,3} \leftarrow (0\,0\,0)3_{3,0}$	300	3000	S. N. Mikhailenko et al. (2018)
213,248,005,986.5 ± 1.7	0.02	$(2\,0\,0)3_{2,2} \leftarrow (0\,0\,0)3_{3,1}$	1.5	5.2	R. Tóbiás et al. (2020)
213,317,003,150.6 ± 1.8	0.02	$(2\,0\,0)5_{0,5} \leftarrow (0\,0\,0)5_{1,4}$	1.2	7.6	M. L. Diouf et al. (2022b)
213,376,695,569.3 ± 1.3	0.02	$(2\,0\,0)4_{1,4} \leftarrow (0\,0\,0)4_{2,3}$	–7.3	8.2	R. Tóbiás et al. (2024)
213,394,923,797.3 ± 1.4	0.02	$(2\,0\,0)6_{5,2} \leftarrow (0\,0\,0)7_{4,3}$	5.2	2.4	R. Tóbiás et al. (2020)
213,446,816,436.0 ± 1.6	0.02	$(2\,0\,0)3_{2,1} \leftarrow (0\,0\,0)3_{3,0}$	2.5	2.4	R. Tóbiás et al. (2020)
213,511,286,802.5 ± 1.4	0.02	$(2\,0\,0)4_{2,2} \leftarrow (0\,0\,0)4_{3,1}$	4.8	12.1	R. Tóbiás et al. (2024)
213,526,600,994.6 ± 1.6	0.02	$(2\,0\,0)6_{2,4} \leftarrow (0\,0\,0)6_{3,3}$	0.4	5.1	R. Tóbiás et al. (2024)
213,534,197,981.2 ± 1.5	0.02	$(2\,0\,0)5_{4,2} \leftarrow (0\,0\,0)6_{3,3}$	1.6	7.5	M. L. Diouf et al. (2022b)
213,539,473,234.3 ± 1.5	0.02	$(2\,0\,0)3_{2,2} \leftarrow (0\,0\,0)4_{1,3}$	–1.1	5.1	R. Tóbiás et al. (2024)
213,663,124,477.7 ± 2.0	0.01	$(2\,0\,0)2_{0,2} \leftarrow (0\,0\,0)3_{1,3}$	2.8	7.6	R. Tóbiás et al. (2024)
213,670,408,312.7 ± 1.4	0.02	$(0\,2\,1)6_{5,1} \leftarrow (0\,0\,0)5_{5,0}$	–1300	3000	S. N. Mikhailenko et al. (2018)
213,731,119,700.4 ± 0.7	0.02	$(2\,0\,0)6_{3,3} \leftarrow (0\,0\,0)7_{2,6}$	–14.6	11.9	R. Tóbiás et al. (2024)
213,810,471,367.1 ± 1.9	0.02	$(2\,0\,0)3_{1,3} \leftarrow (0\,0\,0)3_{2,2}$	0.9	5.3	R. Tóbiás et al. (2020)
213,917,346,155.5 ± 1.8	0.02	$(2\,0\,0)5_{4,1} \leftarrow (0\,0\,0)6_{3,4}$	0.3	7.5	M. L. Diouf et al. (2022b)
214,699,466,014.1 ± 1.8	0.01	$(2\,0\,0)4_{4,0} \leftarrow (0\,0\,0)5_{3,3}$	1.5	3.2	R. Tóbiás et al. (2024)
215,226,610,741.4 ± 1.7	0.02	$(2\,0\,0)4_{2,2} \leftarrow (0\,0\,0)5_{1,5}$	8.7	10.4	R. Tóbiás et al. (2024)
215,262,964,876.7 ± 1.7	0.02	$(2\,0\,0)3_{2,1} \leftarrow (0\,0\,0)4_{1,4}$	6.7	8.0	R. Tóbiás et al. (2024)
215,412,696,377.0 ± 1.2	0.02	$(2\,0\,0)5_{2,3} \leftarrow (0\,0\,0)6_{1,6}$	0.5	7.5	M. L. Diouf et al. (2022b)
215,524,549,225.1 ± 1.7	0.02	$(1\,0\,1)5_{2,3} \leftarrow (0\,0\,0)4_{4,0}$	2.6	2.6	R. Tóbiás et al. (2020)
215,531,118,312.8 ± 1.9	0.01	$(2\,0\,0)2_{2,0} \leftarrow (0\,0\,0)3_{1,3}$	3.7	2.4	R. Tóbiás et al. (2020)
215,854,572,219.6 ± 2.1	0.02	$(2\,0\,0)5_{1,5} \leftarrow (0\,0\,0)4_{2,2}$	4.4	7.7	M. L. Diouf et al. (2022b)
215,968,528,397.7 ± 1.7	0.02	$(2\,0\,0)4_{2,3} \leftarrow (0\,0\,0)3_{3,0}$	12.4	4.9	R. Tóbiás et al. (2024)
216,021,042,445.5 ± 1.6	0.02	$(2\,0\,0)4_{1,4} \leftarrow (0\,0\,0)3_{2,1}$	–7.6	4.9	R. Tóbiás et al. (2024)
216,269,473,019.8 ± 1.4	0.02	$(1\,0\,1)4_{3,1} \leftarrow (0\,0\,0)5_{1,4}$	0.5	5.3	R. Tóbiás et al. (2020)
216,320,509,854.1 ± 1.3	0.02	$(0\,0\,2)4_{1,4} \leftarrow (0\,0\,0)5_{2,3}$	500	3000	S. N. Mikhailenko et al. (2018)
216,467,935,089.8 ± 1.9	0.02	$(2\,0\,0)4_{2,2} \leftarrow (0\,0\,0)3_{3,1}$	7.2	4.9	R. Tóbiás et al. (2024)
216,766,816,926.4 ± 1.9	0.02	$(1\,0\,1)5_{2,3} \leftarrow (0\,0\,0)6_{0,6}$	4.5	2.4	R. Tóbiás et al. (2020)
216,815,183,206.7 ± 4.6	0.01	$(2\,0\,0)2_{0,2} \leftarrow (0\,0\,0)1_{1,1}$	–0.8	9.5	R. Tóbiás et al. (2024)
216,913,210,411.2 ± 1.7	0.02	$(2\,0\,0)6_{3,4} \leftarrow (0\,0\,0)7_{0,7}$	–3.1	3.1	R. Tóbiás et al. (2024)
216,943,217,125.0 ± 1.8	0.01	$(2\,0\,0)2_{2,0} \leftarrow (0\,0\,0)2_{1,1}$	2.9	5.6	R. Tóbiás et al. (2020)
217,353,416,776.9 ± 1.4	0.02	$(2\,0\,0)5_{2,3} \leftarrow (0\,0\,0)4_{3,2}$	16.5	11.4	R. Tóbiás et al. (2024)
217,533,265,067.6 ± 1.5	0.02	$(2\,0\,0)3_{2,2} \leftarrow (0\,0\,0)3_{1,3}$	3.4	5.5	R. Tóbiás et al. (2020)
217,680,819,618.1 ± 1.7	0.01	$(1\,0\,1)5_{2,3} \leftarrow (0\,0\,0)5_{2,4}$	3.0	6.5	R. Tóbiás et al. (2024)
217,893,962,755.6 ± 1.5	0.02	$(2\,0\,0)3_{1,3} \leftarrow (0\,0\,0)2_{0,2}$	–0.8	5.2	R. Tóbiás et al. (2020)
218,089,528,336.1 ± 1.4	0.02	$(2\,0\,0)5_{2,4} \leftarrow (0\,0\,0)5_{1,5}$	8.6	7.9	R. Tóbiás et al. (2024)
218,300,740,560.6 ± 1.5	0.02	$(2\,0\,0)4_{4,0} \leftarrow (0\,0\,0)4_{3,1}$	1.5	5.2	R. Tóbiás et al. (2020)
218,430,303,226.9 ± 0.6	0.02	$(2\,0\,0)6_{2,5} \leftarrow (0\,0\,0)6_{1,6}$	3.2	7.5	M. L. Diouf et al. (2022b)
218,683,177,038.4 ± 1.4	0.02	$(2\,0\,0)2_{2,0} \leftarrow (0\,0\,0)1_{1,1}$	3.5	5.2	R. Tóbiás et al. (2020)
219,622,319,932.4 ± 1.4	0.02	$(2\,0\,0)5_{2,4} \leftarrow (0\,0\,0)4_{1,3}$	2.4	7.6	M. L. Diouf et al. (2022b)
219,863,156,322.3 ± 0.7	0.02	$(2\,0\,0)6_{2,5} \leftarrow (0\,0\,0)5_{1,4}$	7.3	11.2	R. Tóbiás et al. (2024)
219,952,878,188.5 ± 1.4	0.02	$(0\,0\,2)4_{1,4} \leftarrow (0\,0\,0)5_{0,5}$	900	3000	S. N. Mikhailenko et al. (2018)

Notes.
[a] New Lamb-dip frequencies, with their standard (NIST/SEMATECH 2012) uncertainties, at pressures displayed in column "p." The nine italicized frequencies were recorded at Amsterdam in 2024, while the other positions were measured at Louvain-la-Neuve in 2025.
[b] The rovibrational assignments are given as $(v_1'\ v_2'\ v_3')J'_{K_a',K_c'} \leftarrow (v_1''\ v_2''\ v_3'')J''_{K_a'',K_c''}$ (see also Section 2).
[c] Best literature results, corresponding to previous (Lamb-dip and Doppler-limited) experimental line positions or taken from a SNAPS analysis performed in R. Tóbiás et al. (2024). The column "Dev." lists the deviations of the previous frequency values from those reported in the first column. The column "Unc." contains standard uncertainties provided in the cited publications. The deviations, apart from the two underlined cases, remain within the claimed expanded (2σ) uncertainties (NIST/SEMATECH 2012).

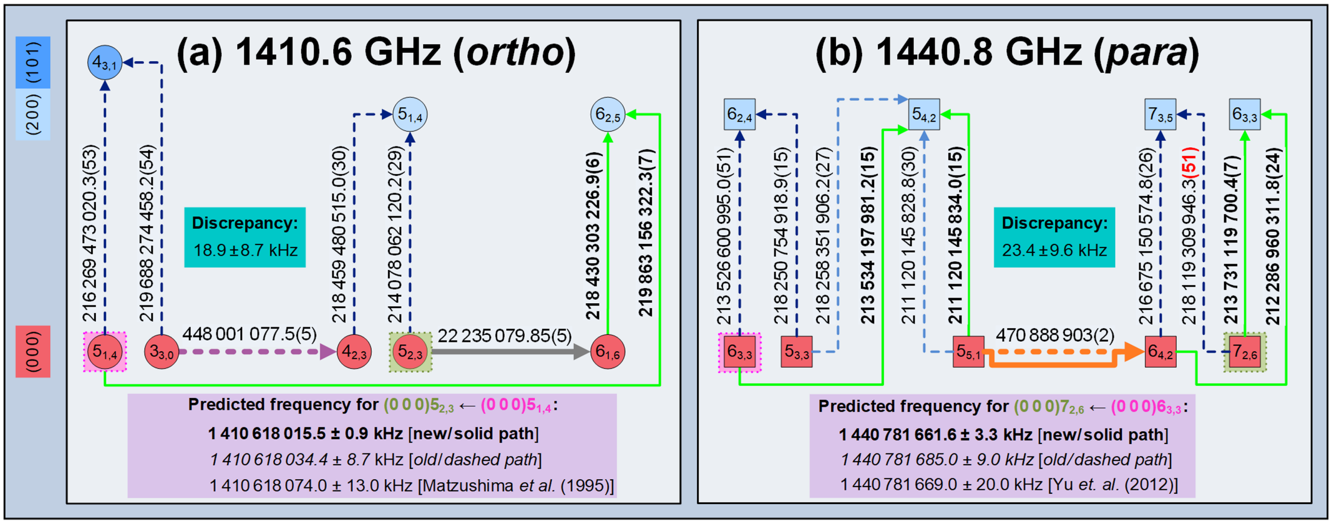

Figure 2. Comparison of new and previous kHz-accuracy paths for two selected radio lines of Table 2. The ortho and para states of this figure are designated with circles and squares, respectively. For these energy levels, the J_{K_a,K_c} labels are written out explicitly, while the (v_1, v_2, v_3) triplets are shown in the left-side color legend. The green arrows denote new Lamb-dip transitions, while those in dark blue, gray, orange, purple, and light blue are extremely accurate lines collected from R. Tóbiás et al. (2020), S. G. Kukolich (1969), G. Y. Golubiatnikov et al. (2006), G. Cazzoli et al. (2009), and W. Ubachs et al. (2024), respectively. For the pure rotational transitions included on the paths, the arrows are thickened. The numbers on the arrows are frequencies in kHz, with the standard NIST/SEMATECH (2012) uncertainties of the last digits in parentheses. The solid arrows constitute the new (smallest-uncertainty) paths between their starting and ending states, surrounded by dotted magenta and green boxes, respectively. The red uncertainty value was slightly underestimated in R. Tóbiás et al. (2020); the true uncertainty must be around 15 kHz. The dashed arrows represent the previous paths, forming cycles with the solid ones. The orange line, illustrated as a double arrow, is part of both paths. The rest frequencies, related to lines between the starting and ending states of the two paths, are placed at the top of both panels. The mauve and teal boxes provide predicted frequencies and discrepancies, along with their standard uncertainties, respectively. The direct experimental values are also listed in the mauve boxes. These two examples correspond to the highest improvements achieved for the protected ortho- and para-$H_2{}^{16}O$ transitions.

2020; M. L. Diouf et al. 2022b). Since the measurements were carried out at 0.01–0.02 Pa, this led to a pressure-induced uncertainty of 0.2–0.4 kHz. In the final uncertainties, the power-shift and day-to-day errors (0.5 and 1.5 kHz, respectively) were also taken into account.

For the measurement campaign at Louvain-la-Neuve, an automated scanning procedure was implemented, ensuring multiple recordings under stabilized conditions. All these experiments were conducted at 0.02 Pa, averaging over at least 16 scans, which gave rise to deviations typically below 1 kHz. At Louvain-la-Neuve, the frequency-comb laser (Toptica DFC Core+) was locked to a quartz oscillator clock, whose uncertainty was studied in a separate measurement campaign. This contribution is 0.9 kHz for the majority of lines averaged over 16 recordings, a somewhat larger value for averages over eight scans, while for the four lines involved in long-term averaging over 100 scans this clock-related uncertainty becomes negligible. In the total uncertainty budget, the pressure-shift uncertainty, translating to 0.4 kHz at 0.02 Pa, was added as a linear term to the combined statistical (clock plus scan) uncertainty.

Figure 1 shows spectra of two new Lamb dips recorded at Louvain-la-Neuve and fitted using a derivative dispersion function (this model is well suited to wavelength-modulated NICE-OHMS signals). On the bottom panels of Figure 1, the fitting residuals are also plotted, whose oscillating features are ascribed to effects due to the combination of high-frequency modulation with low-frequency wavelength modulation, a phenomenon investigated in detail by J. M. Supplee et al. (1994). These oscillating features are characteristic of using a large modulation depth, where the signal deviates from a pure first-derivative line shape and contains contributions from higher-order derivatives of the dispersion profile. While this complicates a fully analytical description, the symmetry of these contributions ensures that their effect on the determination of the line frequency is negligible. Note that the verification cycles, listed in Table S3, also show that the new lines are consistent within the claimed uncertainties.

The list of 55 lines, measured during this study for $H_2{}^{16}O$, is presented in Table 1, where the nine frequencies recorded in Amsterdam are typeset in italics. The typical accuracy of the new measurements is around 2 kHz, thereby improving upon our previous experimental (R. Tóbiás et al. 2020; M. L. Diouf et al. 2022b) or SNAPS-predicted (R. Tóbiás et al. 2024) line-center positions. For eight transitions, only Doppler-broadened observations were previously available, with a claimed uncertainty of 3 MHz (S. N. Mikhailenko et al. 2018).

4. Network-based Frequency Predictions

The ultraprecise $H_2{}^{16}O$ network, augmented with the newly measured lines presented in Table 1, was used to extract highly accurate frequencies for radio lines. Figure 2 illustrates how the predicted frequencies have been extended from this network, applying the Ritz principle (W. Ritz 1908) in a successive fashion.

In these examples, a connection has to be made between opposite-parity levels in the ground vibrational state, and an odd number of known rotational lines must be included. The first nine IAU/CRAF transitions, see Table 2, which were measured at an accuracy better than 1 kHz in microwave studies (S. G. Kukolich 1969; G. Y. Golubiatnikov et al. 2006; G. Cazzoli et al. 2009), serve this purpose. This extreme precision could be achieved only for one SNAPS prediction, see Figure 2(a), relying on two of the four sub-kHz-accuracy lines reported in Table 1.

For the remaining 51 lines in Table 2, all part of the IAU/CRAF and NAS lists, the frequencies could be improved, on

Table 2
Improved Frequencies for Protected $H_2{}^{16}O$ Lines Provided in the IAU/CRAF and NAS Lists

Line Frequency		Rovibrational Assignment[b]	24SNAPS[d,e]		Best Measured[c,e]		
Rest[a] (GHz)	Recommended[b,e] (kHz)		Dev.	Unc.	Dev.	Unc.	Reference
22.235	*22,235,079.85 ± 0.05*	$(0\,0\,0)6_{1,6} \leftarrow (0\,0\,0)5_{2,3}$	0	0.05	0	0.05	S. G. Kukolich (1969)
183.310	*183,310,087.0 ± 1.0*	$(0\,0\,0)3_{1,3} \leftarrow (0\,0\,0)2_{2,0}$	0	1.0	0	1	G. Y. Golubiatnikov et al. (2006)
325.153	*325,152,899.0 ± 1.0*	$(0\,0\,0)5_{1,5} \leftarrow (0\,0\,0)4_{2,2}$	0	1.0	0	1	G. Y. Golubiatnikov et al. (2006)
380.197	*380,197,359.8 ± 0.1*	$(0\,0\,0)4_{1,4} \leftarrow (0\,0\,0)3_{2,1}$	0	0.1	0	0.1	G. Cazzoli et al. (2009)
439.151	*439,150,794.8 ± 0.3*	$(0\,0\,0)6_{4,3} \leftarrow (0\,0\,0)5_{5,0}$	0	0.3	0	0.3	G. Cazzoli et al. (2009)
448.001	*448,001,077.5 ± 0.5*	$(0\,0\,0)4_{2,3} \leftarrow (0\,0\,0)3_{3,0}$	0	0.5	0	0.5	G. Cazzoli et al. (2009)
474.689	*474,689,108.0 ± 1.0*	$(0\,0\,0)5_{3,3} \leftarrow (0\,0\,0)4_{4,0}$	0	1.0	0	1	G. Y. Golubiatnikov et al. (2006)
556.936	*556,935,987.7 ± 0.3*	$(0\,0\,0)1_{1,0} \leftarrow (0\,0\,0)1_{0,1}$	0	0.3	0	0.3	G. Cazzoli et al. (2009)
620.700	*620,700,954.9 ± 0.6*	$(0\,0\,0)5_{3,2} \leftarrow (0\,0\,0)4_{4,1}$	0	0.6	0	0.6	G. Cazzoli et al. (2009)
752.033	752,033,122.7 ± 3.5	$(0\,0\,0)2_{1,1} \leftarrow (0\,0\,0)2_{0,2}$	0	8.2	−19	13	F. Matsushima et al. (1995)
916.172	916,171,449.4 ± 2.7	$(0\,0\,0)4_{2,2} \leftarrow (0\,0\,0)3_{3,1}$	0.5	8.3	−44	13	F. Matsushima et al. (1995)
970.315	970,315,041.5 ± 3.5	$(0\,0\,0)5_{2,4} \leftarrow (0\,0\,0)4_{3,1}$	3.6	9.4	−73	18	F. Matsushima et al. (1995)
987.927	987,926,790.7 ± 3.3	$(0\,0\,0)2_{0,2} \leftarrow (0\,0\,0)1_{1,1}$	0.6	7.9	−48	16	F. Matsushima et al. (1995)
1097.365	1,097,364,863.4 ± 5.4	$(0\,0\,0)3_{1,2} \leftarrow (0\,0\,0)3_{0,3}$	−0.8	6.4	−72	13	F. Matsushima et al. (1995)
1113.343	1,113,343,013.8 ± 4.8	$(0\,0\,0)1_{1,1} \leftarrow (0\,0\,0)0_{0,0}$	0.2	7.1	−50	16	F. Matsushima et al. (1995)
1153.127	1,153,126,821.0 ± 4.4	$(0\,0\,0)3_{1,2} \leftarrow (0\,0\,0)2_{2,1}$	−0.8	6.3	1	13	F. Matsushima et al. (1995)
1158.324	1,158,323,846.3 ± 7.3	$(0\,0\,0)6_{3,4} \leftarrow (0\,0\,0)5_{4,1}$	0	7.3	−103	25	F. Matsushima et al. (1995)
1162.912	1,162,911,605.0 ± 2.6	$(0\,0\,0)3_{2,1} \leftarrow (0\,0\,0)3_{1,2}$	1.1	8.7	−12	13	F. Matsushima et al. (1995)
1207.639	1,207,638,697.3 ± 2.2	$(0\,0\,0)4_{2,2} \leftarrow (0\,0\,0)4_{1,3}$	−2.2	8.2	17	13	F. Matsushima et al. (1995)
1228.789	1,228,788,725.2 ± 2.8	$(0\,0\,0)2_{2,0} \leftarrow (0\,0\,0)2_{1,1}$	−0.8	6.2	47	13	F. Matsushima et al. (1995)
1322.065	1,322,064,738.5 ± 5.4	$(0\,0\,0)6_{2,5} \leftarrow (0\,0\,0)5_{3,2}$	0	5.4	65	13	F. Matsushima et al. (1995)
1410.618	1,410,618,015.5 ± 0.9	$(0\,0\,0)5_{2,3} \leftarrow (0\,0\,0)5_{1,4}$	18.9	8.7	58	13	F. Matsushima et al. (1995)
1440.782	1,440,781,661.6 ± 3.3	$(0\,0\,0)7_{2,6} \leftarrow (0\,0\,0)6_{3,3}$	23.4	9.0	7	20	S. Yu et al. (2012)
1541.967	1,541,967,023.2 ± 3.3	$(0\,0\,0)6_{3,3} \leftarrow (0\,0\,0)5_{4,2}$	−3.2	9.7	−238	23	F. Matsushima et al. (1995)
1602.219	1,602,219,231.7 ± 3.4	$(0\,0\,0)4_{1,3} \leftarrow (0\,0\,0)4_{0,4}$	4.5	8.0	−50	16	F. Matsushima et al. (1995)
1661.008	1,661,007,733.5 ± 4.0	$(0\,0\,0)2_{2,1} \leftarrow (0\,0\,0)2_{1,2}$	0	4.0	−96	22	F. Matsushima et al. (1995)
1669.905	1,669,904,804.7 ± 3.0	$(0\,0\,0)2_{1,2} \leftarrow (0\,0\,0)1_{0,1}$	0	3.0	−30	37	F. Matsushima et al. (1995)
1713.883	1,713,883,014.3 ± 2.7	$(0\,0\,0)4_{3,2} \leftarrow (0\,0\,0)5_{0,5}$	−14.5	9.7	−41	13	F. Matsushima et al. (1995)
1716.770	1,716,769,691.1 ± 4.2	$(0\,0\,0)3_{0,3} \leftarrow (0\,0\,0)2_{1,2}$	0	4.2	−58	13	F. Matsushima et al. (1995)
1716.957	1,716,956,809.3 ± 2.7	$(0\,0\,0)5_{3,3} \leftarrow (0\,0\,0)6_{0,6}$	1.9	3.7	−20	50	S. Yu et al. (2013)
1762.043	1,762,042,823.3 ± 4.6	$(0\,0\,0)6_{3,3} \leftarrow (0\,0\,0)6_{2,4}$	−0.4	6.7	−32	13	F. Matsushima et al. (1995)
1794.789	1,794,788,968.0 ± 4.6	$(0\,0\,0)6_{2,4} \leftarrow (0\,0\,0)6_{1,5}$	0.7	6.8	−15	13	F. Matsushima et al. (1995)
1867.749	1,867,748,648.3 ± 2.5	$(0\,0\,0)5_{3,2} \leftarrow (0\,0\,0)5_{2,3}$	−4.8	5.1	−54	13	F. Matsushima et al. (1995)
1880.753	1,880,752,561.9 ± 3.2	$(0\,0\,0)6_{3,4} \leftarrow (0\,0\,0)7_{0,7}$	−4.3	8.7	39	50	S. Yu et al. (2012)
1893.687	1,893,686,479.5 ± 3.5	$(0\,0\,0)3_{3,1} \leftarrow (0\,0\,0)4_{0,4}$	1.9	8.0	33	50	S. Yu et al. (2012)
1918.485	1,918,485,320.0 ± 1.8	$(0\,0\,0)5_{2,3} \leftarrow (0\,0\,0)4_{3,2}$	16.0	8.6	4	16	F. Matsushima et al. (1995)
1919.360	1,919,359,453.6 ± 2.6	$(0\,0\,0)3_{2,2} \leftarrow (0\,0\,0)3_{1,3}$	−0.9	5.6	77	13	F. Matsushima et al. (1995)
2014.865	2,014,864,766.5 ± 3.0	$(0\,0\,0)5_{4,2} \leftarrow (0\,0\,0)6_{1,5}$	5.1	9.8	95	50	S. Yu et al. (2013)
2040.477	2,040,476,837.9 ± 2.4	$(0\,0\,0)4_{3,1} \leftarrow (0\,0\,0)4_{2,2}$	3.9	6.3	−28	20	F. Matsushima et al. (1995)
2074.432	2,074,432,379.7 ± 3.3	$(0\,0\,0)4_{1,3} \leftarrow (0\,0\,0)3_{2,2}$	5.4	9.3	−75	16	F. Matsushima et al. (1995)
2164.132	2,164,131,934.9 ± 2.3	$(0\,0\,0)3_{1,3} \leftarrow (0\,0\,0)2_{0,2}$	−0.8	5.5	45	18	F. Matsushima et al. (1995)
2196.346	2,196,345,798.7 ± 2.1	$(0\,0\,0)3_{3,0} \leftarrow (0\,0\,0)3_{2,1}$	−0.3	6.6	−43	16	F. Matsushima et al. (1995)
2221.751	2,221,750,318.8 ± 2.1	$(0\,0\,0)5_{1,4} \leftarrow (0\,0\,0)5_{0,5}$	−17.4	9.7	181	18	F. Matsushima et al. (1995)
2264.150	2,264,149,516.4 ± 2.1	$(0\,0\,0)4_{2,3} \leftarrow (0\,0\,0)4_{1,4}$	−0.3	6.6	134	13	F. Matsushima et al. (1995)
2344.290	2,344,250,440.9 ± 6.6	$(0\,0\,0)7_{2,5} \leftarrow (0\,0\,0)7_{1,6}$	0	6.6	−106	18	F. Matsushima et al. (1995)
2365.900	2,365,899,627.5 ± 3.4	$(0\,0\,0)3_{3,1} \leftarrow (0\,0\,0)3_{2,2}$	2.8	9.4	31	20	F. Matsushima et al. (1995)
2391.573	2,391,572,601.6 ± 2.6	$(0\,0\,0)4_{0,4} \leftarrow (0\,0\,0)3_{1,3}$	0	2.6	26	13	F. Matsushima et al. (1995)
2462.933	2,462,933,063.0 ± 2.3	$(0\,0\,0)4_{3,2} \leftarrow (0\,0\,0)4_{2,3}$	−4.2	7.5	−31	13	F. Matsushima et al. (1995)
2630.960	2,630,959,501.0 ± 2.6	$(0\,0\,0)5_{3,3} \leftarrow (0\,0\,0)5_{2,4}$	0.4	7.1	19	27	F. Matsushima et al. (1995)
2640.474	2,640,473,835.2 ± 5.6	$(0\,0\,0)4_{1,4} \leftarrow (0\,0\,0)3_{0,3}$	−6.7	6.8	−22	3	B. J. Drouin et al. (2011)
2657.666	2,657,665,709.0 ± 2.4	$(0\,0\,0)4_{4,1} \leftarrow (0\,0\,0)5_{1,4}$	14.0	8.1	81	50	K. V. Chance et al. (1998)
2664.561	2,664,570,686.1 ± 2.8	$(0\,0\,0)7_{4,3} \leftarrow (0\,0\,0)7_{3,4}$	−2.6	9.3	18	16	F. Matsushima et al. (1995)
2685.639	2,685,638,980.4 ± 2.7	$(0\,0\,0)5_{2,4} \leftarrow (0\,0\,0)5_{1,5}$	7.1	7.8	−11	18	F. Matsushima et al. (1995)
2773.977	2,773,976,550.5 ± 2.7	$(0\,0\,0)2_{2,1} \leftarrow (0\,0\,0)1_{1,0}$	0	2.7	38	20	F. Matsushima et al. (1995)
2880.025	2,880,025,391.7 ± 3.9	$(0\,0\,0)6_{3,4} \leftarrow (0\,0\,0)6_{2,5}$	−1.1	7.6	−23	30	F. Matsushima et al. (1995)
2884.279	2,884,278,943.9 ± 3.2	$(0\,0\,0)6_{1,5} \leftarrow (0\,0\,0)6_{0,6}$	−0.4	6.6	−4	18	F. Matsushima et al. (1995)
2884.941	2,884,941,050.2 ± 2.9	$(0\,0\,0)6_{4,2} \leftarrow (0\,0\,0)6_{3,3}$	6.3	7.0	2	18	F. Matsushima et al. (1995)
2962.111	2,962,111,102.6 ± 4.3	$(0\,0\,0)6_{2,4} \leftarrow (0\,0\,0)5_{3,3}$	−1.6	4.6	−9	16	F. Matsushima et al. (1995)

Table 2
(Continued)

Line Frequency		Rovibrational Assignment[b]	24SNAPS[d,e]		Best Measured[c,e]		
Rest[a] (GHz)	Recommended[b,e] (kHz)		Dev.	Unc.	Dev.	Unc.	Reference
2968.749	2,968,748,638.6 ± 2.6	$(0\,0\,0)2_{2,0} \leftarrow (0\,0\,0)1_{1,1}$	−0.2	5.8	15	16	F. Matsushima et al. (1995)
2970.800	2,970,800,363.7 ± 2.3	$(0\,0\,0)5_{1,4} \leftarrow (0\,0\,0)4_{2,3}$	−3.3	7.6	−120	16	F. Matsushima et al. (1995)

Notes.
[a] Approximate ("rest") frequencies extracted from the primary and supplementary IAU/CRAF reference lists (below 1 THz) or the NAS catalog (above 1 THz). The 2631.051 and 2970.801 GHz frequencies, which correspond to the same rovibrational transitions as the 2630.960 and 2970.800 GHz values, respectively, are not included in this table.
[b] Recommended transition frequencies ± standard (NIST/SEMATECH 2012) uncertainties, derived in the present work via the SNAPS scheme and attached with their rovibrational assignments. Most of these values rely on the new Lamb-dip frequencies given in Table 1.
[c] The most accurate laboratory measurements taken from the literature. The sixth column ("Dev.") contains the deviations of the measured positions from the recommended frequencies. The seventh column ("Unc.") includes the standard uncertainties taken from the individual data sources. The experimental position of the 2640.474 GHz line, reported in B. J. Drouin et al. (2011), does not reflect the zero-pressure value, as it was recorded at a pressure higher than 100 Pa, without pressure correction.
[d] SNAPS estimates utilizing the previous version of the ultraprecise $H_2{}^{16}O$ network considered in W. Ubachs et al. (2024).
[e] The recommended frequencies typeset in italics fully coincide with their direct experimental counterparts, leading to zero deviations in the sixth ("Dev.") column. Similarly, where zero deviations are reported in the fourth ("Dev.") column, the recommended values do not benefit from the newly measured Lamb dips.

average, by a factor of 3, with respect to our previous SNAPS analysis (R. Tóbiás et al. 2024), and even better when compared to the direct THz measurements (F. Matsushima et al. 1995; K. V. Chance et al. 1998; B. J. Drouin et al. 2011; S. Yu et al. 2012). The new network-assisted measurements made it possible to utilize the sub-kHz-accuracy near-infrared transition of S. Kassi et al. (2022), yielding an uncertainty of 2.6 kHz for the 1163 GHz line. For a comparison of the frequency estimates available for the protected $H_2{}^{16}O$ lines (C. H. Townes & F. R. Merritt 1946; S. Golden et al. 1948; C. K. Jen 1951; W. C. King & W. Gordy 1954; S. G. Kukolich 1969; D. A. Stephenson & R. G. Strauch 1970; C. Huiszoon 1971; G. Steenbeckeliers & J. Bellet 1971; F. C. de Lucia et al. 1972; J.-M. Flaud et al. 1972; J. W. Fleming & M. J. Gibson 1976; J. Kauppinen et al. 1978; J. Kauppinen & E. Kyrö 1980; R. H. Partridge 1981; A. V. Burenin et al. 1983; P. Helminger et al. 1983; J. K. Messer et al. 1983; J. W. C. Johns 1985; G. Guelachvili & K. N. Rao 1986; A. Bauer et al. 1989; V. N. Markov & A. F. Krupnov 1995; F. Matsushima et al. 1995; L. R. Brown & C. Plymate 1996; A. Bauer et al. 1998; K. V. Chance et al. 1998; L. H. Coudert et al. 2004; G. Y. Golubiatnikov 2005; G. Y. Golubiatnikov et al. 2006; M. A. Koshelev et al. 2007; G. Cazzoli et al. 2009; B. J. Drouin et al. 2011; M. A. Koshelev 2011; S. Yu et al. 2012; M. Y. Tretyakov et al. 2013; S. Yu et al. 2013; L. H. Coudert et al. 2014; S. N. Mikhailenko et al. 2020; R. Tóbiás et al. 2020; M. L. Diouf et al. 2022b; M. Toureille et al. 2022; E. V. Karlovets et al. 2024; S. N. Mikhailenko et al. 2024), see the online supplemental information.

It should be stressed that all transition frequencies included in the ultraprecise $H_2{}^{16}O$ network relate to zero-pressure values, either through (i) measurements at very low (0.01–0.02 Pa) pressures, (ii) explicit extrapolation to zero pressure, or (iii) including the possible pressure-shift effects in the uncertainty budget. Hence, the listed values for the protected radio lines also pertain to zero-pressure values, with special relevance for the extremely low pressures in interstellar space.

5. Conclusion

In the present study, an ultraprecise spectroscopic network, corresponding to quantum states and transitions of the $H_2{}^{16}O$ water isotopologue has been extended and refined by the precise frequency calibration of 55 rovibrational transitions determined using the NICE-OHMS measurement technology. Of the 60 radio lines protected by the International Astronomical Union and the Panel on Frequency Allocations of the US National Academy of Sciences, 51 have been considerably improved in accuracy due to our present and previous Lamb-dip positions. Specifically, their uncertainties, falling into the 10–200 kHz range, have been brought to below 7.5 kHz. For the nine lowest-frequency transitions, all known with an accuracy better than 1 kHz, no improvements could be achieved. These lines play an essential role within the network, because they connect the even- and odd-parity levels of the ground vibrational state.

In principle, a similar analysis might be conducted for $H_2{}^{18}O$ as well. A large database of Lamb-dip lines has already been collected (M. L. Diouf et al. 2021), and a partial procedure for extracting radio lines from this database has been executed previously (W. Ubachs et al. 2024). For the HDO isotopologue, such a procedure was halted in view of parity-pair-mixing effects that limited the accuracy of the Lamb dips measured in M. L. Diouf et al. (2022a).

Supplemental Information

Additional data related to this work are available at doi:10.5281/zenodo.16757167. Table S1 contains a list of new experimental $H_2{}^{16}O$ rovibrational transitions recorded for the present paper with the NICE-OHMS technique at Amsterdam and Louvain-la-Neuve. Table S2 provides the paths within the ultraprecise $H_2{}^{16}O$ network for all radio lines given in Table 2, the best paths defining radio frequencies, as well as the collection of data sources used in the comparison. Table S3 includes basic cycles associated with the shortest-path-based forest of the ultraprecise $H_2{}^{16}O$ network.

Acknowledgments

This work was funded by LASERLAB-EUROPE (grant No. 654148), a European Union Horizon 2020 research and innovation program. The present study is part of a European Partnership on a Metrology project, which is cofinanced by the European Union's Horizon Europe Research and Innovation Programme and by the Participating States (funder ID: 10.13039/100019599, grant No.: 23FUN04 COMOMET). The research performed in Budapest received support from the National Research, Development and Innovation Office of Hungary (NKFIH, grants K138233 and PD145972). A.A., A. B., and C.L. acknowledge the FNRS CDR (grant No. J.0113.23) and MIS (grant No. F.4038.24) for financial support. We also thank the LAS&O technological platform for the use of the frequency comb at Louvain.

ORCID iDs

Arthémise Altman https://orcid.org/0009-0000-3924-3497
Roland Tóbiás https://orcid.org/0000-0003-3674-5066
Alexandr S. Bogomolov https://orcid.org/0000-0002-6675-0969
Meissa L. Diouf https://orcid.org/0000-0003-1262-6003
Frank M. J. Cozijn https://orcid.org/0000-0002-8169-5961
Attila G. Császár https://orcid.org/0000-0001-3674-191X
Clément Lauzin https://orcid.org/0000-0001-5044-5137
Wim Ubachs https://orcid.org/0000-0001-7840-3756

References

Bauer, A., Godon, M., Carlier, J., & Gamache, R. 1998, JQSRT, 59, 273
Bauer, A., Godon, M., Kheddar, M., & Hartmann, J. 1989, JQSRT, 41, 49
Brown, L. R., & Plymate, C. 1996, JQSRT, 56, 263
Burenin, A. V., Fevralskikh, T. M., Karyakin, E. N., Polyansky, O. L., & Shapin, S. M. 1983, JQSRT, 100, 182
Cazzoli, G., Puzzarini, C., Harding, M. E., & Gauss, J. 2009, CPL, 473, 21
Cazzoli, G., Puzzarini, C., & Lapinov, A. 2004, ApJ, 611, 615
Cernicharo, J., Goicoechea, J. R., Daniel, F., et al. 2006, ApJ, 649, L33
Chance, K. V., Park, K., & Evenson, K. M. 1998, JQSRT, 59, 687
Chen, J., Hua, T.-P., Tao, L.-G., et al. 2018, JQSRT, 205, 91
Cheung, A. C., Rank, D. M., Townes, C. H., Thornton, D. D., & Welch, W. J. 1969, Natur, 221, 626
Committee on Radio Frequencies Board on Physics and Astronomy, National Academies of Sciences–Engineering–Medicine 2015, Handbook of Frequency Allocations and Spectrum Protection for Scientific Uses (Washington, DC: National Academy of Sciences)
Coudert, L. H., Martin-Drumel, M.-A., & Pirali, O. 2014, JMoSp, 303, 36
Coudert, L. H., Pirali, O., Vervloet, M., Lanquetin, R., & Camy-Peyret, C. 2004, JMoSp, 228, 471
Cozijn, F. M. J., Dupré, P., Salumbides, E. J., Eikema, K. S. E., & Ubachs, W. 2018, PhRvL, 120, 153002
Császár, A. G., & Furtenbacher, T. 2011, JMoSp, 266, 99
de Lucia, F. C., Helminger, P., Cook, R. L., & Gordy, W. 1972, PhRvA, 5, 487
Diouf, M. L., Tóbiás, R., Cozijn, F. M. J., et al. 2022a, OExpr, 30, 46040
Diouf, M. L., Tóbiás, R., Simkó, I., et al. 2021, JPCRD, 50, 023106
Diouf, M. L., Tóbiás, R., van der Schaaf, T. S., et al. 2022b, MolPh, 120, e2050430
Drouin, B. J., Yu, S., Pearson, J. C., & Gupta, H. 2011, JMoSt, 1066, 2
Endres, C. P., Schlemmer, S., Schilke, P., Stutzki, J., & Müller, H. S. P. 2016, JMoSp, 327, 95
Flaud, J.-M., Camy-Peyret, C., & Valentin, A. 1972, JPhys, 33, 741
Fleming, J. W., & Gibson, M. J. 1976, JMoSp, 62, 326
Furtenbacher, T., Tóbiás, R., Tennyson, J., Polyansky, O. L., & Császár, A. G. 2020a, JPCRD, 49, 033101
Furtenbacher, T., Tóbiás, R., Tennyson, J., et al. 2020b, JPCRD, 49, 043103
Gianfrani, L., Hu, S.-M., & Ubachs, W. 2024, NCimR, 47, 229
Golden, S., Wentink, T., Hillger, R., & Strandberg, M. W. P. 1948, PhRv, 73, 92
Golubiatnikov, G. Y. 2005, JMoSp, 230, 196
Golubiatnikov, G. Y., Markov, V. N., Guarnieri, A., & Knochel, R. 2006, JMoSp, 240, 251
Guelachvili, G., & Rao, K. N. 1986, Handbook of Infrared Standards (Orlando, FL: Academic Press)
Helminger, P., Messer, J. K., & de Lucia, F. C. 1983, ApPhL, 42, 309
Huiszoon, C. 1971, RScI, 42, 477
Jen, C. K. 1951, PhRv, 81, 197
Johns, J. W. C. 1985, OSAJB, 2, 1340
Karlovets, E. V., Mikhailenko, S. N., Koroleva, A. O., & Campargue, A. 2024, JQSRT, 314, 108829
Kassi, S., Lauzin, C., Chaillot, J., & Campargue, A. 2022, PCCP, 24, 23164
Kassi, S., Stoltmann, T., Casado, M., Daeron, M., & Campargue, A. 2018, JChPh, 148, 054201
Kauppinen, J., Kärkkäinen, T., & Kyrö, E. 1978, JMoSp, 71, 15
Kauppinen, J., & Kyrö, E. 1980, JMoSp, 84, 405
King, W. C., & Gordy, W. 1954, PhRv, 93, 407
Koshelev, M. A. 2011, JQSRT, 112, 550
Koshelev, M. A., Tretyakov, M. Y., Golubiatnikov, G. Y., et al. 2007, JMoSp, 241, 101
Kukolich, S. G. 1969, JChPh, 50, 3751
Markov, V. N., & Krupnov, A. F. 1995, JMoSp, 172, 211
Matsushima, F., Odashima, H., Iwasaki, T., Tsunekawa, S., & Takagi, K. 1995, JMoSp, 352, 371
Messer, J. K., de Lucia, F. C., & Helminger, P. 1983, IJIMW, 4, 505
Miani, A., & Tennyson, J. 2004, JChPh, 120, 2732
Mikhailenko, S. N., Béguier, S., Odintsova, T. A., et al. 2020, JQSRT, 253, 107105
Mikhailenko, S. N., Karlovets, E. V., Koroleva, A. O., & Campargue, A. 2024, JPCRD, 53, 023102
Mikhailenko, S. N., Mondelain, D., Karlovets, E. V., Kassi, S., & Campargue, A. 2018, JQSRT, 206, 163
Müller, H. S. P., Schlöder, F., Stutzki, J., & Winnewisser, G. 2005, JMoSt, 742, 215
NIST/SEMATECH 2012, e-Handbook of Statistical Methods (NIST/SEMATECH) https://www.itl.nist.gov/div898/handbook/mpc/section5/mpc57.htm
Partridge, R. H. 1981, JMoSp, 87, 429
Pickett, H., Poynter, R., Cohen, E., et al. 1998, JQSRT, 60, 883
Ritz, W. 1908, ApJ, 28, 237
Solomon, P., & Klemperer, W. 1972, ApJ, 178, 389
Steenbeckeliers, G., & Bellet, J. 1971, CRASB, 273, 471
Stephenson, D. A., & Strauch, R. G. 1970, JMoSp, 35, 494
Supplee, J. M., Whittaker, E. A., & Lenth, W. 1994, ApOpt, 33, 6294
Tielens, A., & Hagen, W. 1982, A&A, 114, 245
Tóbiás, R., Diouf, M. L., Cozijn, F. M., Ubachs, W., & Császár, A. G. 2024, CmChe, 7, 34
Tóbiás, R., Furtenbacher, T., Simkó, I., et al. 2020, NatCo, 11, 1708
Toureille, M., Koroleva, A. O., Mikhailenko, S. N., Pirali, O., & Campargue, A. 2022, JQSRT, 291, 108326
Townes, C. H., & Merritt, F. R. 1946, PhRv, 70, 558
Tretyakov, M. Y., Koshelev, M. A., Vilkov, I. N., Parshin, V. V., & Serov, E. A. 2013, JQSRT, 114, 109
Ubachs, W., Császár, A. G., Diouf, M. L., Cozijn, F. M., & Tóbiás, R. 2024, ESC, 8, 1901
van Dishoeck, E. F., Herbst, E., & Neufeld, D. A. 2013, ChRv, 113, 9043
Weiß, A., De Breuck, C., Marrone, D. P., et al. 2013, ApJ, 767, 88
Wright, C. M., van Dishoeck, E. F., Black, J. H., et al. 2000, A&A, 358, 689
Yu, S., Pearson, J. C., & Drouin, B. J. 2013, JMoSp, 288, 7
Yu, S., Pearson, J. C., Drouin, B. J., et al. 2012, JMoSp, 279, 16